Aerodynamic Effects on Wind Turbulence Measurements with Research Aircraft

JOHN A. KALOGIROS* AND QING WANG

Department of Meteorology, Naval Postgraduate School, Monterey, California

(Manuscript received 1 May 2001, in final form 27 March 2002)

ABSTRACT

Flow distortion is a major issue in the measurement of wind turbulence with gust probes mounted on a nose boom, at the radome, or under the wing of research aircraft. In this paper, the effects both of the propellers of a turboprop aircraft and of the aircraft vortex system on the pressure and wind velocity measurements near the nose of the aircraft are examined. It is shown that, for a turboprop aircraft, the sensors mounted near the nose are affected directly (slipstream) or indirectly (lift increase) by the propellers. The propeller effects are more significant for pressure sensors located ahead of the propellers on the fuselage and are less significant for the small local flow angles measured at the nose of the aircraft. The first case is clearly realized during in-flight calibration maneuvers performed by a turboprop aircraft. A major flow distortion, which seriously affects the vertical wind velocity measurements near the nose of an aircraft, is the upwash induced mainly by the wing-bound vortex. Also, low energy of the vertical wind component in the inertial subrange for scales larger than the fuselage diameter is usually observed in aircraft measurements. This is shown to be the result of not taking into account the decrease of the upwash correction with eddy frequency (or no need for such a correction in the inertial subrange) caused by the aerodynamic delay and the response of the wing vortex to turbulence. The level of energy in the inertial subrange of the vertical wind component is significant because it is commonly used for the estimation of the dissipation rate of turbulence kinetic energy. A method to estimate this frequency variable correction and correct the spectra or the time series of the estimated vertical wind component is described. Data from low-level flight legs with a Twin Otter aircraft show that this correction may result in about a 20% correction of the variance of the vertical wind component and a 5% correction of the vertical turbulent fluxes.

1. Introduction

Research aircraft are extensively used to probe the wind turbulence field in the atmospheric boundary layer. They have the advantage over stationary measurement stations of sampling a large area of the usually inhomogeneous wind field. However, they require high-frequency and very accurate measurements of both airstream and aircraft ground velocity components (Lenschow 1986), which are possible now at low cost with the advances in the involved technology. In addition, the wings, the fuselage, and the propellers or the jet engines of the aircraft cause flow distortion, which is different for each aircraft and decreases with the distance ahead of the aircraft. Even in the case of using a long boom at the nose of the aircraft to mount the sensors (Crawford and Dobosy 1992), the flow distortion (mainly that due to the wing effect) is still significant (Crawford et al. 1996). In-flight calibration maneuvers are typically used to estimate the flow distortion and to compute corrections for the wind measurements (Lenschow 1986; Bögel and Baumann 1991; Tjernström and Friehe 1991; Khelif et al. 1999; Kalogiros and Wang 2002).

During calibration maneuvers, the acceleration of the aircraft from changes in engine thrust is significant (typically 1–2 m s^{-2}) and the flow around the aircraft is different from normal flight conditions. The change of the flow around the aircraft may be attributed to the difference between accelerating (unsteady) and steady airflow (Williams and Marcotte 2000). This raises the question of whether a complicated calibration of the wind measurement system dependent on aircraft acceleration should be used, even though this acceleration is small (but its variations may be significant) during normal flight conditions. However, the unsteadiness effect of longitudinal acceleration (with no pitch oscillation of the aircraft) on the flow around the aircraft relative to a steady-state flow with the same instantaneous free airstream speed is governed by the ratio of acceleration multiplied by a characteristic length scale of the body that distorts the flow (e.g., the fuselage diameter or the wing chord) to the square of the ambient speed of sound

* Current affiliation: Institute of Environmental Research and Sustainable Development, National Observatory of Athens, Athens, Greece.

Corresponding author address: Dr. J. Kalogiros, Institute of Environmental Research and Sustainable Development, National Observatory of Athens, I. Metaxa and Vas. Pavlou, Lofos Koufou, GR 15236, P. Penteli, Athens, Greece.
E-mail: jkalog@meteo.noa.gr

FIG. 1. Photograph of the CIRPAS Twin Otter showing the arrangement of the radome, the static pressure ports (starboard side), and the wind–propeller system.

(Bisplinghoff and Ashley 1975). This is because the flow perturbations propagate with the speed of sound. The above ratio is very small for typical acceleration values of research aircraft, and, thus, we may suspect that the observed change of the pressure and flow fields near the nose of the aircraft during acceleration is mainly due to engine effects.

The vertical wind component is very significant because it is used for the computation of the vertical turbulent fluxes with eddy correlation methods and the estimation of the dissipation rate of turbulence kinetic energy by inertial subrange spectral methods from aircraft data (Nicholls and Readings 1981; Durand et al. 1991). The vertical wind component measured with an aircraft is seriously affected by the flow distortion created by the aircraft. The upwash induced by the wing-bound vortex (the vortex attached to the wing) may be modeled using the lifting-line aerodynamic wing theory. Such a simple model for the upwash near the nose of an aircraft has been described by Crawford et al. (1996) along with corrections for various research aircraft, which are similar in value, with estimated corrections obtained by in-flight calibration maneuvers. However, as they note, that model is applicable for large turbulent length scales. The power spectrum of the vertical wind component obtained from research aircraft wind measurements (corrected for the upwash effect using the results of calibration maneuvers) at small length scales usually shows low energy when compared with the spectra of the other wind components (Nicholls and Readings 1981; Tjernström and Friehe 1991; Lenschow et al. 1991). Thus, although the local isotropy power law of $-5/3$ is observed in the inertial subrange of the power spectrum of the vertical wind component, its ratio with the power spectrum of the longitudinal component along the sampling direction is lower than the expected isotropic value of 4/3 (Kaimal and Finnigan 1994). The corresponding ratio for the case of the lateral component is found to be close to this value. The sampling direction in the case of a moving platform (aircraft) is the airstream direction.

In this paper, we examine first the effects of the propellers on pressure and flow-angle sensors located near the nose of a turboprop research aircraft during significant changes in aircraft acceleration caused by changes in propeller thrust, as is the case during speed run maneuvers. Then, we examine the response of the wing to turbulence and its effect on high-frequency measurements of the vertical wind component. The data used in this paper were obtained during the Development and Evolution of Coastal Stratocumulus experiment in June and July 1999 off the coast of Monterey, California, with a two-engine Twin Otter (model series 300) research aircraft operated by the Center for Interdisciplinary Remote Piloted Aircraft Study (CIRPAS) of the Naval Postgraduate School. Details on the aircraft, its instrumentation, and the calibration of the wind measurement system are given by Kalogiros and Wang (2002).

2. Propeller effects near the nose of an aircraft

On research aircraft, many sensors are located near the nose. On the CIRPAS Twin Otter, the static pressure ports and the Pitot tube that measures the dynamic pressure are located on the fuselage just in front of the cockpit, and the wind measurement system (radome pressure probe) is located at the aircraft's nose (Fig. 1).

These sensors are very close to the propellers of the aircraft, and it is possible that changes in engine thrust (especially during calibration maneuvers) affect their measurements. A propeller affects the flow ahead of it directly or indirectly. The direct effect is the suction effect, which is more significant within the slipstream (the tube of high speed that includes the streamlines passing through the propeller disk). The indirect effect is an increase of the upwash induced by the vortex of the wing part behind the propeller and within the slipstream. This is due to the increase of the speed of the oncoming flow at that part of the wing causing an increase of the local vortex circulation and lift. In our simple approach below, we do not analyze the very complex interaction of the propeller with the nacelle and wing located downstream of the propeller. The presence of the wing alters (because of the upwash) the angle of the incident flow on the propeller (Koning 1963) and is of secondary importance relative to the effect of the propeller alone. The effect of the swirl (tangential air velocity) introduced in the slipstream by the propeller is to cause nearly symmetrical changes of the local attack angle with opposite sign on each side of the propeller axis and, thus, has a small net result (Aljabri and Hughes 1985).

We used the analytical model of Koning (1963), which approximates the propeller as an actuator disk (momentum theory) with a sudden pressure drop on it and uses the potential theory (no viscosity outside the boundary layer of the aircraft or compressibility effects) to calculate the pressure and air velocity fields in front of and behind the propeller. The solution equations describing the flow field structure can be found in Koning (1963). According to this model, for a given geometry (dimensions and positions of the propellers), the flow field depends on two parameters: the free airstream speed and the axial interference factor (or equivalently the thrust coefficient) of the propeller. The axial interference factor is the relative increase of axial air velocity through the propeller disk, and the thrust coefficient is defined as the ratio of thrust force to the product of propeller disk area and dynamic pressure of the free airstream. Thus, if measurements of the change of pressure relative to the static pressure of the free airstream at a point close to the propeller are available, the model can be used to estimate the axial interference factor. This estimation is then used to calculate the flow field deviation and wing vortex circulation change due to the propeller.

We used the measurement of the static pressure port located on the fuselage ahead of the propellers. According to the analysis in Kalogiros and Wang (2002), the static pressure defect at the position of the static pressure port during the speed run maneuvers depended on the acceleration (or equivalently on engine thrust) of the aircraft (see Fig. 2). Using their Eq. (2), the effects of dynamic pressure and flow angles on the static pressure defect were removed. The resulting static pressure

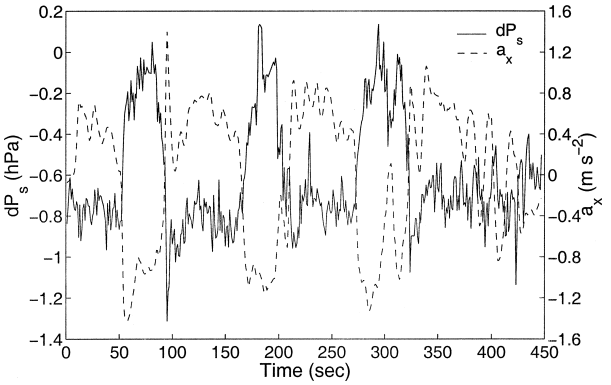

FIG. 2. The pressure change dP_s at the position of the static pressure port due to the propeller effect for the speed run maneuver on 22 Jul 1999. The longitudinal acceleration of the aircraft a_x estimated from the time derivative of the differential GPS aircraft ground velocity is also shown.

defect, with an addition of a possible offset so that it is about zero during the deceleration of the aircraft (very low thrust), is the change of pressure at the position of the static pressure port due to the propeller thrust. The result of this procedure for the speed run maneuver on 22 July 1999 is shown in Fig. 2 along with the longitudinal acceleration of the aircraft. The axial interference factor of the propellers was estimated by inverting Koning's model as mentioned above. The diameter of each of the two propellers of the Twin Otter is about 2.6 m, and their axes are located on the wing 2.8 m from the centerline of the aircraft. The position of the static pressure ports relative to the propeller axis is about 2.0 m in the longitudinal direction of the aircraft, 2.1 m in the lateral direction, and 1.0 m in the vertical direction. The corresponding coordinates for the center of the radome at the nose of the aircraft are 3.7, 2.8, and 1.2 m, respectively. Close to the fuselage, the lateral velocity component of the flow (the velocity component perpendicular to the fuselage surface) will decrease to a near-zero value (nonentry condition). When this velocity component was forced to zero in the analytical model of Koning, the change of the pressure field was found to be very small. This is expected since the change in the longitudinal (along the free airstream) component is the most important factor in pressure change according to the Bernoulli equation. Thus, our estimates of pressure change and the axial interference factor of the propeller should not be affected significantly by the fuselage effect.

Figure 3 shows the vertical component of the measured upwash at the nose of the aircraft calculated using the measured local flow angles at the radome and the wind equations for the same time period as in Fig. 2. In this calculation we assumed a zero vertical wind velocity at the area of the maneuvers (above the atmospheric boundary layer). Figure 3 also shows the estimated upwash (total modeled) and its components at the same position. These components are the upwash

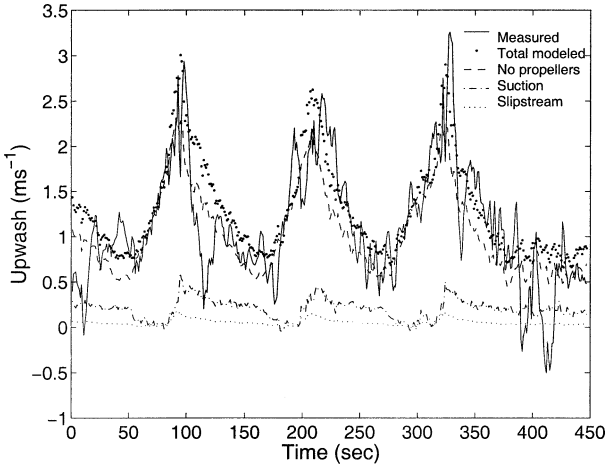

FIG. 3. The vertical component of the measured upwash at the nose of the aircraft, and the estimated upwash (total modeled) and its components for the same time period as in Fig. 2.

induced by the various parts of the aircraft except the propellers (no propellers), the suction effect of the propellers (suction), and the additional upwash due to the increase of the vortex circulation at the wing part behind the propellers (slipstream).

The first component includes the effects of the wing-bound vortex (which is the most significant effect), the trailing vortices shed in the wake of the wing (which are more significant at the wingtips), and the fuselage. An accurate estimation of these effects requires modeling of the whole aircraft (using computational fluid dynamics numerical models or potential theory panel methods) because of the interaction among them. Such a complex and computer-time-demanding modeling is not within the objectives of this paper but rather to provide an answer to the question of whether there is a measurable effect of the propellers at the nose of the aircraft. We used a simpler vortex lattice method (Bertin and Smith 1998), which is an extension of the lifting-line method, to model the effects of the wing-bound and trailing vortices during deceleration (small propeller effects). The wing area of the Twin Otter is about 39 m^2, the wing span is 19.8 m, and the wing chord is 2.0 m. The longitudinal distance and the vertical distances from the nose to the aerodynamic center of the wing (the point at 1/4 of the chord length from the leading edge of the wing where the lift force acts) are about 5.7 and 1.1 m, respectively. The estimated upwash at the radome was consistently about one-half of the measured upwash, with their ratio slightly decreasing with an increasing angle of attack, and the lift was reproduced within 5% difference. The measured lift was calculated from acceleration measurements as discussed in the paragraph following Eq. (1) below. The difference between the modeled-as-above and the measured upwash is probably due to the interaction of the wing vortices with the fuselage, which is more significant close to the fuselage. This is similar to the increase of local air velocity due to the thickness (fineness ratio) of the fuselage, which is included as the body form factor in the estimation of the parasite drag of the aircraft (Shevell 1989). It can also be interpreted as near cancellation of the downwash induced by the wingtip vortices at the nose of the aircraft (this is about 35% of the upwash induced there by the wing-bound vortex) due to their interaction with the fuselage (Katz and Plotkin 2001).

Thus, we preferred to use a more direct method to model the induced upwash at the radome with no propeller effects. Since this upwash component should be proportional to the free airstream speed and the difference between the local attack angle and the free airstream angle of attack, we used the deceleration data (small propeller effects) to construct a regression model of this dependence. A similar method was used to model the lift dependence on the free airstream speed and angle of attack. The propellers' direct and indirect effects at the nose of the aircraft are the superposition (potential theory) of the corresponding effects of both symmetrically positioned propellers. The suction effect at the radome and the increase of the flow speed over the wing part behind the propellers was estimated with Koning's model using the axial interference factor already found by the analysis of static pressure variations. The local average increase of the vortex circulation at the wing part inside the slipstream during acceleration of the aircraft was calculated from the departure of the lift from the modeled value mentioned above and the Kutta–Joukowski theorem (Bertin and Smith 1998). The relative increase of circulation was modeled as proportional to the relative increase of the local flow speed (Koning 1963). The additional upwash at the radome due to a horseshoe vortex (since, according to the Helmholtz vortex theorems, a vortex filament cannot end in the fluid) with that circulation was then estimated using the Biot–Savart law. In our calculation we also took into account the interaction with the fuselage, which was found to increase by about 2 times the upwash near the fuselage as mentioned above. Figure 4 shows the measured and modeled changes of the vortex circulation at the wing part inside the slipstream for the speed run maneuver on 17 July 1999, which was characterized by less noise from the acceleration measurements as compared with the 22 July 1999 maneuver. The close agreement between measured and modeled values except at the peak values (near stall) confirms that the increase in circulation is due to the propellers' slipstream.

According to Fig. 3, the vortex-induced upwash component due to the increase of the speed of the airstream in the slipstream behind the propellers is very small. The main components are the upwash induced by the wing and, to a lesser extent, the suction by the propellers. The latter effect brings the values of the estimated upwash during acceleration periods (especially the peak values) closer to the measured upwash. The disagreement in the details between modeled and measured upwash and some small negative values are probably due

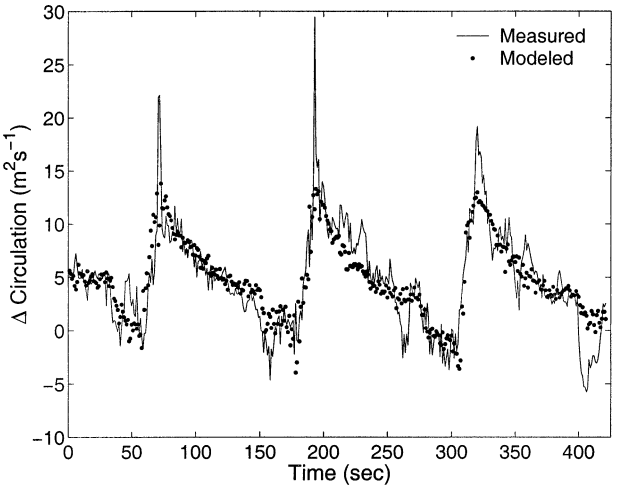

FIG. 4. Measured and modeled change of the vortex circulation at the wing part inside the slipstream for the speed run maneuver on 17 Jul 1999.

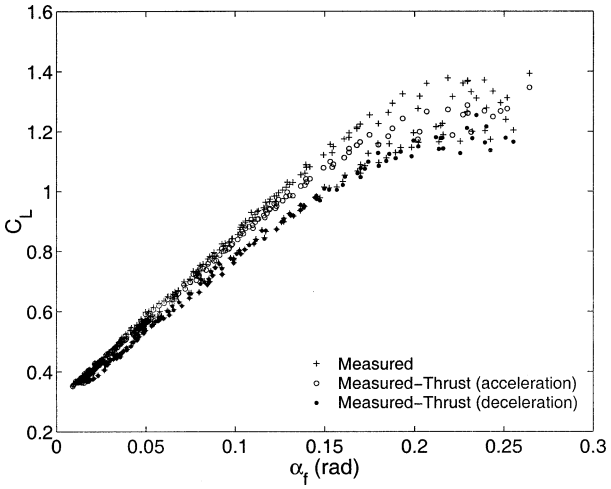

FIG. 5. The lift coefficient C_L vs the angle of attack α_f of the free airstream for the speed run maneuver on 17 Jul 1999. The lift coefficient with the thrust component removed is also shown.

to the sensitivity of the measurements to errors of the radome attack differential pressure. The angle of attack calculated from the modeled upwash using the wind equations and with an assumption of zero vertical wind velocity at the area of the maneuvers (not shown here) showed a small loop behavior when plotted against the free airstream angle of attack. This was not discernible in the case of the measured angle of attack because of the scatter of the data. According to Fig. 3, this small loop corresponds to a difference of about 0.25 m s^{-1} on average and peak values of 0.5 m s^{-1} relative to the case with no propeller effects. The sideslip angle measurements should not be affected by the suction of the propellers because of their symmetrical position relative to the nose of the aircraft.

Figure 5 shows the lift coefficient C_L against the attack angle of the free airstream (lift curve) for the speed run maneuver on 17 July 1999 for the same time period as in Fig. 4. The lift coefficient C_L is the ratio of the aerodynamic force perpendicular to the free airstream per wing area (wing loading) to the dynamic pressure of the free airstream:

$$C_L = \frac{ma_n}{P_d S}, \tag{1}$$

where m is the mass of the aircraft, P_d is the dynamic pressure of free airstream, S is the wing area, and a_n is the component of the acceleration of the aircraft perpendicular to the free airstream. The lift coefficient was calculated using slow (1 Hz) acceleration measurements (the time derivative of the differential GPS aircraft ground velocity data). The average gross weight of the aircraft was estimated to be about 4900 kg. The measured lift included the lift due to the wing with no propeller effects, the thrust component perpendicular to the free airstream, and the increase in lift due to the propellers' slipstream. Figure 5 also shows the lift coefficient calculated after removing the thrust component. The lift curve shows that the acceleration part of the plot (decreasing α_f) has a higher lift coefficient C_L and the deceleration part (increasing α_f) has lower C_L. Each part shows a linear lift curve up to 0.15 rad (8.6°) with a 5.5796 and 4.7624 rad^{-1} slope value for the acceleration and the deceleration, respectively. The corresponding zero lift angles of attack are −0.0532 and −0.0630 rad. A −2.5° (−0.0436 rad) value for the zero lift angle and similar values of lift of coefficient have been reported for the Twin Otter by Norment (1988) and Drummond and MacPherson (1985). Using the above-estimated slope of the lift curve for the deceleration case, which includes relatively small effects of the propellers, and the simple model of the upwash effect by Crawford et al. (1996), a 0.835 value of the slope coefficient of the calibration of the angle of attack is obtained (see the discussion of Fig. 7a in section 3 below). This value is very close to the value of 0.814 estimated by Kalogiros and Wang (2002) using calibration maneuvers. Figure 5 shows that the loop behavior of measured C_L is mostly due to the additional lift by the propellers' slipstream and less to the corresponding thrust component.

The results of the above analysis of the departure of measured static pressure, upwash at the radome, and lift during acceleration of the aircraft from their corresponding values during deceleration support the idea that they are due to the propeller effects. Thus, we may conclude that the observed dependence of the airflow on aircraft acceleration during calibration maneuvers is mainly due to the propeller effects (especially the suction effect) and not to unsteady flow effects caused by the longitudinal acceleration of the flow. As can be seen from the method of analysis, the exact level of the propellers' or jet engines' effects on the measurements depends

mainly on the arrangement of the turbulence probes and the engines and the power of the engines.

3. Wing response to turbulence

The vertical wind velocity measured with a gust probe located ahead of the wing is subject to a significant error due to the upwash induced by the aircraft vortex system and is typically estimated from calibration maneuvers. We note that this upwash includes the effects of the wing-bound vortex, the wingtip vortices, and the interaction with the fuselage as discussed in the previous section. However, apparently the effects of the tip vortices at the nose of the aircraft are nearly canceled by the interaction with the fuselage. The upwash model described by Crawford et al. (1996) includes only the effect of the wing-bound vortex and explains the observed upwash in terms of the wing theory, but it is valid for steady flow or low frequencies of turbulence eddies. The wing response to oscillatory motion and turbulence has been the subject of many theoretical and experimental studies (Bisplinghoff and Ashley 1975). Approximate analytical response functions of the lift have been obtained by the unsteady lifting-line theory for incompressible flow. The response of the wing is mainly determined by the effect of vortices shed in the wake of the wing (trailing vortices). Theodorsen's function describes the lift due to sinusoidal oscillatory motions of an airfoil within a uniform airspeed field and Sears's function describes the lift due to encountering a sinusoidal gust traveling in the direction of flight. The corresponding response functions to step, instead of oscillatory, variations are known as Wagner's and Küssner's functions, respectively. Corrections for the finite aspect ratio of a wing and the two-dimensional spanwise structure of turbulence have also been obtained (Jones 1940; Diederich 1958; Filotas 1971; Okubo et al. 1979).

According to the upwash model of Crawford et al. (1996) the induced angle α_u due to upwash at the measurement position ahead of the wing and on the longitudinal axis of the aircraft (the nose of the aircraft in our case) is

$$\alpha_u = k_u(\alpha_f - \alpha_0), \tag{2}$$

where α_f is the free airstream (geometric) angle of attack, α_0 is the zero lift angle of attack, $k_u = (k_0/n)\, dC_L/d\alpha_f$, $n = r/c$, r is the along-airstream distance between the measurement position and the aerodynamic center of the wing, c is the effective chord length of the wing, and $dC_L/d\alpha_f$ is the slope of the lift curve. The factor k_0 in k_u is equal to $1/\pi^2$ for an elliptical wing (characterized by an elliptical chord or circulation distribution in the spanwise direction) but should be a little different in our case of a rectangular planform wing. The measured angle of attack α is simply

$$\alpha = \alpha_f + \alpha_u. \tag{3}$$

In the case of an aerodynamic response to a sinusoidal gust (a single spectral component of turbulence), the slope of the lift curve $dC_L/d\alpha_f$ is given by

$$\frac{dC_L}{d\alpha_f} = 2\pi S_G, \tag{4}$$

where $S_G(k_x, k_y, A)$ is a generalized Sears response function (Filotas 1971), which includes the effect of finite aspect ratio $A = b^2/S$ (b is the wing span and S is the wing area) and the effect of the spanwise structure of turbulence. The wavenumbers k_x and k_y correspond to the along-airstream and spanwise directions, respectively. For an almost rectangular wing, as is the case of the Twin Otter (or generally for wings with small sweep), the Sears function and the effect of the finite aspect ratio are combinations of Bessel functions of reduced frequency $k_c = \omega(c/2)/U_a$, where $\omega = 2\pi f$ is the angular frequency, f is the eddy frequency, and U_a is the average free airstream speed (Filotas 1971). The longitudinal wavenumber k_x is connected to frequency through Taylor's hypothesis ($\omega = k_x U_a$). The effect of spanwise reduction of coherence of turbulence (Kristensen and Jensen 1979) can be described by the approximate analytical function given by Diederich (1958). A simplified version of this function is given by Okubo et al. (1979) and is a combination of Bessel functions of reduced frequency $k_b = \omega(b/2)/U_a$ based on wing span. The theoretical generalized Sears function for steady flow ($k_x = k_y = 0$) is simply the steady-state lifting line result $S_G = A/(A + 2)$. The slope of the calibration of attack angle [this slope is $(1 + k_u)^{-1}$ according to Eqs. (2) and (3)] estimated from calibration maneuvers corresponds to nearly steady conditions because the maneuvers have relative large time periods (larger that 5 s), and, thus, they do not reveal the response of the wing to high-frequency turbulence. The steady-state k_u estimated with this method can give the value of the k_0 factor, which depends on the shape of the wing, if the lift coefficient C_L is measured [see the paragraph following Eq. (7) below].

Another important response effect that affects the measurements of attack angle (or equivalently the vertical wind velocity) at high frequencies is the geometric time delay due to the longitudinal separation Δx (5.3 m in our case) between the measurement position and the leading edge of the wing. According to Taylor's hypothesis, the phase lag at frequency f between the spectral component of the attack angle at the wing (which determines the bound-vortex circulation) and the same spectral component at the measurement position is $2\pi f \Delta x/U_a$. We do not consider the more complicated case of a wing with considerable sweep. We note, also, that the reference point for the response function S_G is the leading edge of the wing. Thus, if we consider a sinusoidal gust with unit amplitude of the form $\alpha_f'(x, t) = e^{ik_x(U_a t - x)}$ propagating from the measurement position ($x = 0$) toward the wing leading edge ($x = \Delta x$), Eqs. (2)–(4) give

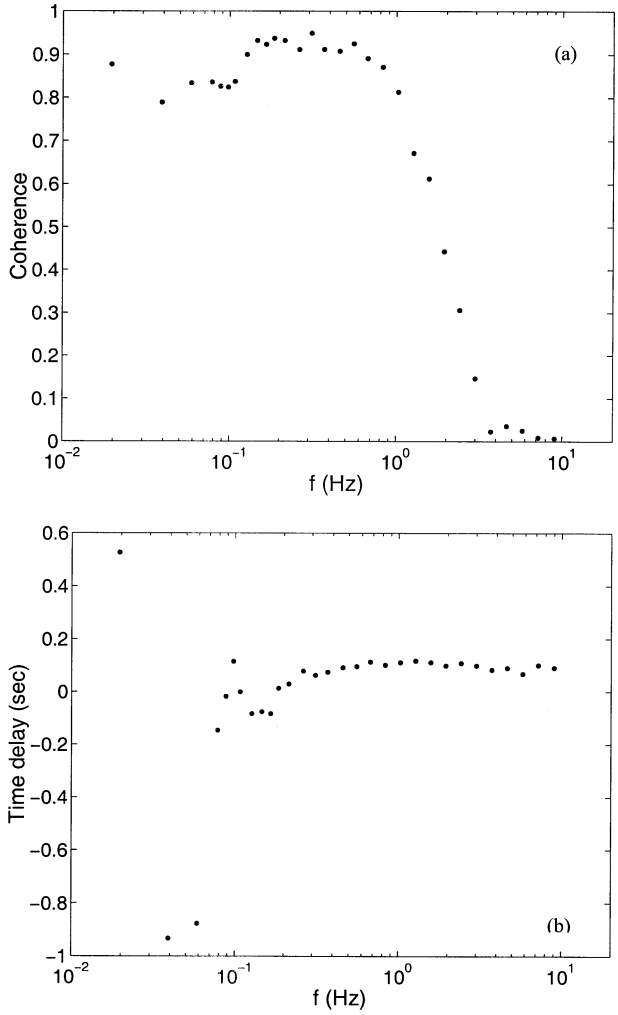

FIG. 6. The frequency content of (a) the coherence and (b) the time delay between measured angle of attack and lift coefficient, respectively, from a 30-km constant-level leg at an altitude of about 36 m above the sea surface on 7 Jul 1999.

$$a'(\Delta x, t) = \frac{a'(0, t)e^{-i2\pi f\Delta x/U_a}}{\left(1 + \frac{2\pi k_0}{n} S_G e^{-i2\pi f\Delta x/U_a}\right)}. \quad (5)$$

The primes denote variations from an average state, x is the longitudinal axis of the aircraft with positive direction downstream, and t is time. Variations of attack angle α_f at Δx are connected to C_L variations according to Eq. (4). Thus, in terms of Fourier transforms,

$$H_{C_L} = 2\pi S_G H_{\alpha_f}, \quad (6)$$

where H denotes Fourier transform of the quantity in the subscript. Using Eqs. (5) and (6), we get

$$\frac{H_{C_L}}{H_\alpha} = \frac{2\pi S_G e^{-i2\pi f\Delta x/U_a}}{\left(1 + \frac{2\pi k_0}{n} S_G e^{-i2\pi f\Delta x/U_a}\right)}. \quad (7)$$

Figures 6a,b show the frequency content of the coherence and the time delay (estimated by the phase lag) between the measured angle of attack and the lift coefficient, respectively, from a 30-km constant-level leg at an altitude of about 36 m above the sea surface on 7 July 1999. The lift coefficient was estimated from Eq. (1). Fast accelerometers were used to measure the three components of the acceleration of the center of gravity of the aircraft. The aircraft acceleration obtained from the differential GPS data in section 2 cannot be used because it is limited to low frequencies. The loss of coherence at low frequencies reflects contributions other than turbulence (control maneuvers by the pilot or the autopilot), and at high frequencies the response of the wing to turbulence drops very quickly. The time delay above 0.4 Hz is almost constant at about 0.1 s, which is the expected time delay according to Eq. (7).

The ratio of the Fourier transforms on the left-hand side of Eq. (7) is equal to the ratio of the cross-spectrum of C_L and α to the power spectrum of α (Bendat and Piersol 1971). Thus, the response function S_G can be estimated from measurements of lift coefficient and attack angle. Figure 7a shows the amplitude of the response function estimated solving Eq. (7) for S_G (measured response) and the theoretical estimation of S_G (Sears function/2D turbulence) as described in the paragraph following Eq. (4) for the same flight leg as in Fig. 6. The factor k_0 in Eq. (7) was chosen to be 1.19 times its value for an elliptical wing ($1/\pi^2$) so that the measured S_G agrees with the theoretical one at low frequencies. Using the value of $dC_L/d\alpha_f$ for the deceleration case during speed run maneuvers (see Fig. 5 and the paragraph at the end of section 2) and the above value of k_0, the steady-state slope $(1 + k_u)^{-1}$ of the calibration of attack angle is 0.835, which is very close to the 0.814 value estimated by the calibration maneuvers. The frequency scale used in Fig. 7a is the reduced frequency k_c based on the half chord, because the Sears function depends on this parameter. We show the measured response function at high frequencies only, because at lower frequencies there are contributions other than turbulence as mentioned above. The phase angle of the response function (not shown) is very small (less than 20°). According to Fig. 7a, the actual effect of the spanwise drop of coherence of turbulence with frequency may be higher than the effect included in the theoretical function. We also include the theoretical wing response for oscillatory motions of the aircraft (Theodorsen function), which shows that, for low-frequency oscillatory motions (such as the ones during aircraft maneuvers, which have a time period longer than 5 s) the departure from steady-state flow is very small. This conclusion holds, also, for the phase spectrum of the response function (not shown). Figure 7b shows the estimated slope of calibration of measured attack angle against frequency using the measured response function S_G. The frequency scale used is the reduced frequency k_b based on the half-wing span, because according to Fig. 7a the

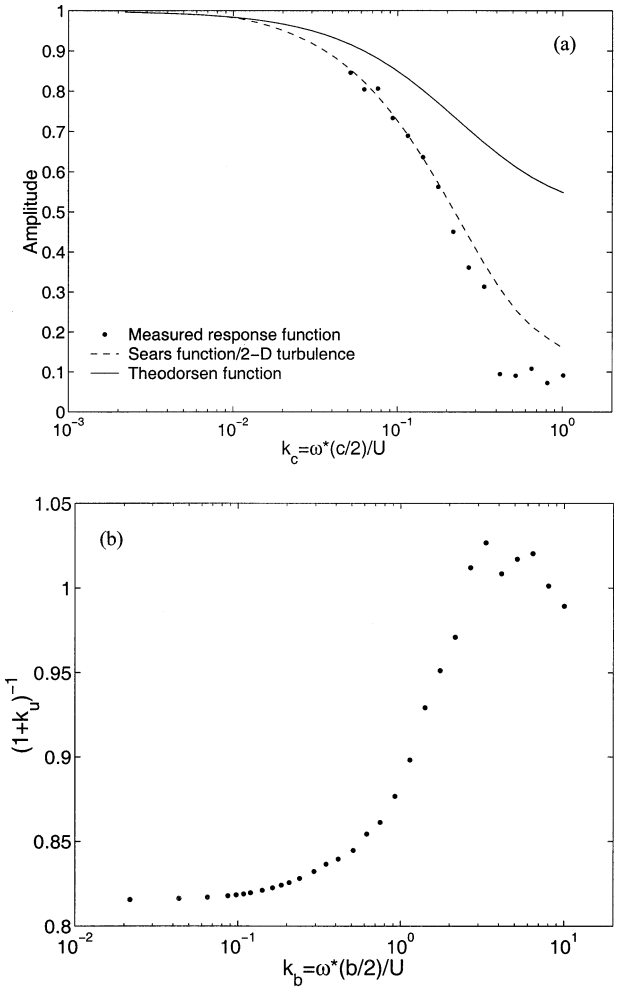

FIG. 7. (a) The amplitude of the measured response function and the theoretical estimation of the generalized Sears function and the Theodorsen function for the same flight leg as in Fig. 6. (b) The estimated slope of calibration of measured attack angle vs frequency using the measured response function S_G for the same flight leg.

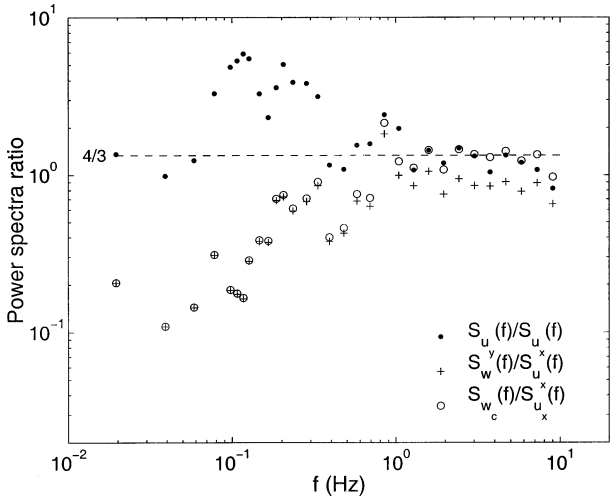

FIG. 8. Ratios of the power spectra of the lateral u_y, the uncorrected vertical w, and the corrected vertical w_c wind components to the power spectrum of the longitudinal wind component u_x (along the average airstream vector) for the same time period as in Figs. 6 and 7. The dashed line is the 4/3 ratio expected from local isotropy in the inertial subrange.

dominant effect in the generalized Sears function is the spanwise loss of coherence of turbulence. The calibration slope increases from the steady-state value to near unity in the inertial subrange within a frequency decade. Thus, the correction is constant with frequency in the inertial subrange and the isotropic $-5/3$ slope of the power spectrum of the vertical wind velocity is not affected. We note that, for wind measurement close to the nose of the aircraft and for the turbulence eddies with scales on the order of the fuselage diameter or smaller (frequencies higher than the 10-Hz maximum frequency shown here), the distortion by the fuselage is significant (Hunt 1973).

The measured response function S_G can be used in Eq. (5) to estimate a frequency response function for the measured attack angle at the measurement position ($x = 0$) and to correct its Fourier transform. This corrected Fourier transform can be used in the calculation of a corrected power spectrum of the vertical wind velocity or its cross-spectra with other quantities. This is justified since the high-frequency variations of vertical wind velocity are proportional to variations of the attack angle. A more accurate approach would be to invert the corrected Fourier transform of the attack angle and to use the resulting corrected time series of the attack angle in the wind equations to compute the wind components. Figure 8 shows power spectra ratios of vertical and lateral wind components to the power spectrum of the longitudinal wind component with respect to the sampling direction (airstream direction) for the same flight leg as in Figs. 6 and 7. This figure is the same as Fig. 14 of Kalogiros and Wang (2002), with the addition of the ratio for the corrected vertical wind velocity. The uncorrected vertical wind velocity was calculated by assuming that the steady-state calibration slope of the attack angle holds for all frequencies. The value of the spectra ratios expected by local isotropy in the inertial subrange is 4/3. Figure 8 shows that the lower energy of the vertical wind velocity relative to the other wind components is not a result of anisotropy but is the result of the wing response to turbulence. We also computed the difference in vertical wind velocity variance and vertical turbulent fluxes of momentum and heat. For the same flight data as those used in Figs. 6, 7, and 8, the result was a 17% increase in vertical wind velocity variance (from 0.218 to 0.254 m^{-2} s^{-2}), a 4% increase in absolute value of momentum flux (from -0.176 to -0.182 m^{-2} s^{-2}), and a 3% increase in heat flux (from 5.31×10^{-3} to 5.48×10^{-3} K m s^{-1}). This difference between the variance and the flux corrections is expected since the contribution of the inertial subrange to the vertical fluxes is very small when compared with the

contribution to the vertical wind velocity variance. Thus, the correction of the vertical wind velocity for the effect of the response of the aircraft vortex system to turbulence may be of practical significance not only for the correct estimation of the dissipation rate of turbulence kinetic energy by inertial subrange spectral methods using aircraft data, but also for the estimation of vertical wind velocity variance and, to a lesser extent, for the vertical turbulent fluxes. We note that the exact percentage of correction is specific to the shape of the vertical velocity spectrum and the aircraft details such as wing dimensions and speed. The method of correction, however, is the same as described here and results in no need for upwash correction in the inertial subrange of the vertical velocity turbulence spectrum.

4. Concluding remarks and discussion

We used a simple model of the propeller to analyze its effect on pressure and in situ wind measurements close to and ahead of the wing of a turboprop aircraft. We found that during aircraft maneuvers the direct suction effect of the propellers is significant for static and dynamic pressure measurements and also for the vertical wind measurements. The effect on the vertical wind measurements should be more significant when the propellers are located higher or lower relative to the position of the gust probe so that a vertical component of the slipstream exists at the probe. The indirect effect of the propellers due to additional lift by the slipstream is less important but may be observed in lift coefficient measurements during maneuvers. During normal straight flight, the engine thrust does not change significantly, and, thus, the propellers should not affect turbulence measurements. Unsteady flow effects due to the longitudinal acceleration of typical research aircraft are too small to affect significantly the flow field near the nose of the aircraft even during maneuvers.

The wing response to turbulence and the delay of interference of the wing with turbulence relative to the wind measurement position have a significant effect on fast measurements of the vertical wind component. The wing response to turbulence can be approximated with considerable accuracy by the theoretical result of the unsteady lifting-line theory. A method to estimate the wing response to turbulence based on in-flight fast acceleration measurements was described. The aerodynamic response correction applied in the frequency or the time domain results in no need for upwash correction and recovery of the isotropic behavior of the vertical wind component in the inertial subrange for scales larger than the fuselage diameter. This is important for the estimation of the dissipation rate of turbulence kinetic energy by inertial subrange spectral methods using aircraft data. The vertical wind velocity variance and, to a lesser extent, the vertical turbulent fluxes are also affected by this correction of vertical wind velocity. Thus, aircraft measurements of vertical wind velocity do not actually show any systematic nonisotropic behavior. The expected isotropic value of 4/3 of the ratio of the power spectra of the lateral and vertical wind component to the longitudinal one (e.g., in the surface layer) could be used to test the calibration of gust probes (or even to calibrate them) on research aircraft.

The exact level of the corrections for the aerodynamic effects discussed in this paper is specific to each aircraft. Thus, we also applied the methods described in this paper to an aircraft very different than the Twin Otter aircraft, the National Center for Atmospheric Research C-130. We used Dynamics and Chemistry of Marine Stratocumulus, Phase II, (DYCOMS-II) field campaign maneuvers and normal flight data. For the analysis of the propeller effects we did not use the speed run maneuvers because they were characterized by smooth acceleration (about 0.5 m s^{-2}) and more rapid deceleration. During the pitch maneuvers, the aircraft acceleration had peak values of more than 1 m s^{-2}, and, thus, the thrust effects were more intense in comparison with the speed run maneuvers. The fuselage static pressure was corrected for altitude variation using the hydrostatic balance assumption and for the dependency of the static pressure defect on flow angles as we did for the Twin Otter in section 2. This dependency was very significant (about 8 times more than the Twin Otter) for the attack angle case. The static pressure changes due to the propeller thrust changes during the pitch maneuvers ranged from near zero at -1 m s^{-2} deceleration to -2.7 hPa at 1 m s^{-2} acceleration. The latter corresponds to a value of about 1.3 m s^{-1} of the vertical component of the airflow due to suction by the propellers and about a 0.5° increase of the local angle of attack at the nose of the aircraft. We note that the suction effect increases the local angle of attack at the nose of the aircraft during the maneuvers, whereas the increase of the dynamic pressure computed from a Pitot tube and the static pressure would result in a decrease of the estimated local angle of attack. However, the latter effect is much smaller than the former. For the analysis of the response of the aircraft vortex system to high-frequency turbulence, we used low-level flight legs (at about 100 m above the sea surface). We found that the coherence between the angle of attack and the lift coefficient falls off rapidly above 1 Hz and that the dependence of the response function on the reduced frequency k_c was close to the theoretical Sears function, as in the Twin Otter case (Figs. 6a and 7a). The estimated slope of the calibration of the measured attack angle goes to unity for values of the reduced frequency k_b greater than 2–3, as in Fig. 7b.

Acknowledgments. This work was sponsored by National Science Foundation Grant ATM9900496.

REFERENCES

Aljabri, A. S., and A. C. Hughes, 1985: Wind tunnel investigation of the interaction of propeller slipstream with nacelle/flap com-

binations. *Proc. AGARD Conf.*, Toronto, ON, Canada, NATO, 21-1–21-10.
Bendat, J. S., and A. G. Piersol, 1971: *Random Data Analysis and Measurement Procedures*. John Wiley and Sons, 407 pp.
Bertin, J. J., and M. L. Smith, 1998: *Aerodynamics for Engineers*. Prentice Hall, 668 pp.
Bisplinghoff, R. L., and H. Ashley, 1975: *Principles of Aeroelasticity*. Dover, 527 pp.
Bögel, W., and R. Baumann, 1991: Test and calibration of the DLR Falcon wind measuring system by maneuvers. *J. Atmos. Oceanic Technol.,* **8,** 5–18.
Crawford, T. L., and R. J. Dobosy, 1992: A sensitive fast-response probe to measure turbulence and heat flux from any airplane. *Bound.-Layer Meteor.,* **59,** 257–278.
——, ——, and E. J. Dumas, 1996: Aircraft wind measurement considering lift-induced upwash. *Bound.-Layer Meteor.,* **80,** 79–94.
Diederich, F. W., 1958: The response of an airplane to random atmospheric turbulence. National Advisory Committee for Aeronautics Rep. 1345, 36 pp.
Drummond, A. M., and J. I. MacPherson, 1985: Aircraft flow effects on cloud drop images and concentrations measured by the NAE Twin Otter. *J. Atmos. Oceanic Technol.,* **2,** 633–643.
Durand, P., L. De Sa, A. Druilhet, and F. Said, 1991: Use of the inertial dissipation method for calculating turbulent fluxes from low-level airborne measurements. *J. Atmos. Oceanic Technol.,* **8,** 78–84.
Filotas, L. T., 1971: Approximate transfer functions for large aspect ratio wings in turbulent flow. *J. Aircr.,* **8,** 395–400.
Hunt, J. C. R., 1973: A theory of turbulent flow round two-dimensional bluff bodies. *J. Fluid Mech.,* **61,** 625–706.
Jones, R. T., 1940: The unsteady lift of a wing of finite aspect ratio. National Advisory Committee for Aeronautics Rep. 681, 8 pp.
Kaimal, J. C., and J. J. Finnigan, 1994: *Atmospheric Boundary Layer Flows: Their Structure and Measurement*. Oxford University Press, 289 pp.
Kalogiros, J. A., and Q. Wang, 2002: Calibration of a radome-differential GPS system on a Twin Otter research aircraft for turbulence measurements. *J. Atmos. Oceanic Technol.,* **19,** 159–171.
Katz, J., and A. Plotkin, 2001: *Low-Speed Aerodynamics*. Cambridge University Press, 613 pp.
Khelif, D., S. P. Burns, and C. A. Friehe, 1999: Improved wind measurements on research aircraft. *J. Atmos. Oceanic Technol.,* **16,** 860–875.
Koning, C., 1963: Influence of the propeller on other parts of the airplane structure. *Aerodynamic Theory,* W. F. Durand, Ed., Vol. IV, Dover, 361–430.
Kristensen, L., and N. O. Jensen, 1979: Lateral coherence in isotropic turbulence and in the natural wind. *Bound.-Layer Meteor.,* **17,** 353–373.
Lenschow, D. H., 1986: Aircraft measurements in the boundary layer. *Probing the Atmospheric Boundary Layer,* D. H. Lenschow, Ed., Amer. Meteor. Soc., 39–55.
——, E. R. Miller, and R. B. Friesen, 1991: A three-aircraft intercomparison of two types of air motion measurements systems. *J. Atmos. Oceanic Technol.,* **8,** 41–50.
Nicholls, S., and C. J. Readings, 1981: Spectral characteristics of the surface layer turbulence over the sea. *Quart. J. Roy. Meteor. Soc.,* **107,** 591–614.
Norment, H. G., 1988: Three-dimensional trajectory analysis of two drop sizing instruments: PMS OAP and PMS FSSP. *J. Atmos. Oceanic Technol.,* **5,** 743–756.
Okubo, H., M. Kobayakawa, and H. Maeda, 1979: Lifting surface approach to the estimation of gust response of finite wings. *J. Aircr.,* **16,** 309–314.
Shevell, R. S., 1989: *Fundamentals of Flight*. Prentice Hall, 438 pp.
Tjernström, M., and C. A. Friehe, 1991: Analysis of a radome air-motion system on a twin-jet aircraft for boundary layer research. *J. Atmos. Oceanic Technol.,* **8,** 19–40.
Williams, A., and D. Marcotte, 2000: Wind measurements on a maneuvering twin-engine turboprop aircraft accounting for flow distortion. *J. Atmos. Oceanic Technol.,* **17,** 795–810.